arXiv:cond-mat/0207455v2 [cond-mat.mes-hall] 17 Feb 2003

Disentangling the exchange coupling of entangled donors in the Si quantum computer architecture

Belita Koiller,[1,2] Xuedong Hu,[1,3] H.D. Drew,[1] and S. Das Sarma[1]

[1] *Condensed Matter Theory Center, Department of Physics, University of Maryland, College Park, MD 20742-4111*

[2] *Instituto de Física, Universidade Federal do Rio de Janeiro, 21945, Rio de Janeiro, Brazil*

[3] *Department of Physics, University at Buffalo, SUNY, Buffalo, NY 14260-1500**

(Dated: February 1, 2008)

We develop a theory for micro-Raman scattering by single and coupled two-donor states in silicon. We find the Raman spectra to have significant dependence on the donor exchange splitting and the relative spatial positions of the two donor sites. In particular, we establish a strong correlation between the temperature dependence of the Raman peak intensity and the inter-donor exchange coupling. Micro-Raman scattering can therefore potentially become a powerful tool to measure interqubit coupling in the development of a Si quantum computer architecture.

PACS numbers: 03.67.Lx, 71.55.Cn, 78.30.-j

Quantum computing has attracted wide-spread interest in recent years [1]. Among many proposed schemes for quantum computer (QC) hardware, a particularly promising architecture is the nuclear spin based Si QC based on donor arrays [2], which has prompted a great deal of activities to study both theoretically and experimentally the fabrication, control, and measurement of such Si-based devices [3, 4, 5, 6, 7, 8, 9, 10, 11]. Currently the fabrication of donor arrays in Si has been pursued using two complementary approaches. The "bottom-up" approach uses low temperature MBE and STM to build the array atom by atom [7], while the "top-down" approach uses ion-implantation [12]. In both approaches, it is crucial to know the precise positions of the donors buried inside the host Si lattice, and to measure the exchange coupling between neighboring donors.

The most important (and daunting from the fabrication perspective of building a Si QC) physical quantity underlying the Si QC architecture is the exchange entanglement of the neighboring donor sites – this exchange coupling must be large enough for two-qubit operations to be possible [2, 3, 4, 5, 6]. Right now, however, there is no proposed method for directly estimating the exchange entanglement in Si, and the experimental fabrication of Si QC architecture is essentially based on the hope of appreciable entanglement in the fabricated devices. In this Letter we not only propose a novel and promising quantitative method for obtaining the exchange coupling in Si donor states based on the easily available technique of electronic micro-Raman spectroscopy [13, 14], but also demonstrate through quantitative calculations the feasibility of our proposed technique as a powerful diagnostic tool for studying buried donor positioning and exchange coupling measurement. Electronic Raman spectroscopy has been widely used to study electronic transitions for which one-photon absorption [15] is forbidden. Furthermore, micro-Raman spectroscopy, with the laser spot size in the order of μm, has the required spatial resolution to provide valuable information on the environment of single donors, pair orientation, and the strength of donor-pair coupling and electronic entanglement. In the following, we develop a theory for micro-Raman scattering from donor electrons in Si, focusing on the situation where photon polarization and sample temperature can be precisely tuned. We show that the electronic micro-Raman spectra have important signatures of donor locations and exchange coupling. We also discuss specific experimental conditions when single donor (or single pair) detection might be possible with this technique.

In Raman scattering (i.e. inelastic light scattering) experiments, an incident laser photon of wave vector $\vec{k}_L$, frequency ω_L and polarization $\vec{\eta}_L$ scatters into a Raman photon with $\vec{k}_R$, ω_R, $\vec{\eta}_R$, while the system with which the radiation interacts undergoes a transition from an initial state $|0\rangle$ of energy E_0 to a final state $|f\rangle$ of energy E_f. The differential Stokes-Raman scattering cross section is given by [16]

$$\frac{d^2\sigma}{d\Omega_R d\omega_R} = \left(\frac{e}{mc}\right)^4 \frac{\omega_R}{\omega_L} \sum_f |M|^2 \delta(\omega - \omega_{f0}) \,, \qquad (1)$$

where $\omega_{f0} = (E_f - E_0)/\hbar$ and $\omega = \omega_L - \omega_R$ is the Raman shift. The matrix element M is written as [16]

$$M = \sum_{\mu,\nu=x,y,z} \eta_L^\mu \eta_R^\nu \left(\frac{\langle f|p_\mu p_\nu|0\rangle}{E_G - \hbar\omega_R} + \frac{\langle f|p_\mu p_\nu|0\rangle}{E_G + \hbar\omega_L} \right) , \qquad (2)$$

where E_G is the direct band gap at the conduction band minimum and $\vec{p}$ is the momentum operator. In Si, the conduction band has six degenerate minima. The lowest donor-electron energy states are a ground-state singlet $1S(A_1)$, and excited triplet $1S(T_2)$ and doublet $1S(E)$ components, consistent with the T_d site symmetry of the substitutional donor [17]. The notation $1S(j)$ refers to a j-symmetry state obtained from 1S-like hydrogenic envelopes, which can be written as [9] $\psi_j(\mathbf{r}) =$

$\sum_{\mu=1}^{6} \alpha_\mu^{(j)} F_\mu(\mathbf{r})\phi_\mu(\mathbf{r})$, where $\phi_\mu(\mathbf{r}) = u_\mu(\mathbf{r})e^{i\mathbf{k}_\mu\cdot\mathbf{r}}$ are Bloch wavefunctions, $F_\mu(\mathbf{r})$ are the hydrogenic envelopes, $\alpha_\mu^{(j)}$ characterize the point group representation, and μ runs over the six conduction band minima $\mathbf{k}_\mu$. Taking this multivalley feature into consideration, Eq. (1) can be simplified [16]:

$$\frac{d^2\sigma}{d\Omega_R d\omega_R} = \left(\frac{e^2}{mc^2}\right)^2 \frac{\omega_R}{\omega_L}\mathcal{R}^2(m_\parallel^{-1} - m_\perp^{-1})^2 \times \left|\sum_{\mu=1}^{6} \alpha_\mu^{(f)*}\alpha_\mu^{(0)}\,(\vec{\eta}_L\cdot\hat{\eta}_\mu)(\vec{\eta}_R\cdot\hat{\eta}_\mu)\right|^2 \delta(\omega-\omega_{f0})\,, \quad (3)$$

where $\mathcal{R}$ is the resonance enhancement factor which, for $\hbar(\omega_L-\omega_R) \ll E_G$, can be expressed as $\mathcal{R} = E_G^2/[E_G^2 - (\hbar\omega_L)^2]$, $m_\parallel$ and $m_\perp$ are the Si conduction band effective masses in units of the free electron mass m, and $\hat{\eta}_\mu$ is the unit vector along the axis of the μth valley.

Electronic Raman scattering in Si:P is dominated by the valley-orbit transition of $1S(A_1) \rightarrow 1S(E)$ states for single donors (the $1S(A_1) \rightarrow 1S(T_2)$ transition is not Raman-active) [16]. The shift and width of the single donor Raman peak can provide donor environment information, since the donor states are sensitive to the local strain fields, the local electric fields from ionized acceptor-donor pairs or surface charge for donors near the surface, and interactions with other neutral donors and acceptors.

To have single donor sensitivity, a micro-Raman experiment needs sufficiently large Raman cross section, which is possible through the resonant Raman effect. The Raman cross section can be estimated neglecting the excitonic effects [18]. In this case the divergence in the resonance enhancement factor $\mathcal{R}$ is limited by the energy level dispersion in the valence band, since the valence bands are not extremal at the conduction band minima. As a result, $\mathcal{R}$ can take on a maximum value of $\mathcal{R}^2 \approx 1000$, leading to a Raman cross section $d\sigma/d\Omega_R \approx 2\times10^{22}$ cm^2/sr. For example, for a laser power of 1 mW the photon flux is 1.6×10^{23} photons/s $\cdot$ cm^2. This leads to a count rate of about 35 s^{-1} per donor, small but workable. In addition, at $T = 10$K and for the incident laser power of 1 mW in a 1 μm spot, the sample temperature rise is estimated to be only 1 K. The spatial resolution needed for micro-Raman experiments is also facilitated by the fact that the resonance condition occurs in the UV ($\sim$ 3.8 eV) where the penetration depth of the radiation is small ($\sim$ 10 nm). For a sample with a donor density of 10^{-16} cm^{-3} and a focal spot size ~ 1 μm there are ~ 100 donors in the field of view. At this density the mean number of donor pairs with separations within 10 nm is about 4.

If resonance enhancement allows sufficiently large signal-to-noise ratio for micro-Raman scattering, an immediate question is what information of the phosphorus donors the Raman spectra carry, and how they are related to donor positions and interdonor coupling. Here we focus on the Raman spectra of a pair of donors at $\mathbf{R}_A$ and $\mathbf{R}_B$ (relative position $\mathbf{R} = \mathbf{R}_A - \mathbf{R}_B$), namely, when the $|0\rangle$ and $|f\rangle$ states of Eq. (2) are two-donor states. It is thus necessary to study the composition and energy spectra of the Raman-active donor-pair states, which is the theory we develop here.

In the limit of distances $|\mathbf{R}|$ much larger than the effective Bohr radii, consistent with the Si QC proposals [2, 3, 4], the two-particle singlet and triplet states within the $1S$ manifold may be written in the Heitler-London (HL) approach:

$$\psi_{s\atop t}^{i,j}(\mathbf{r}_1,\mathbf{r}_2) = \{u[\,|A_1^i,B_2^j\rangle \pm |B_1^j,A_2^i\rangle] + v[\,|A_1^j,B_2^i\rangle \pm |B_1^i,A_2^j\rangle]\}\,(|\uparrow\downarrow\rangle \mp |\downarrow\uparrow\rangle) \quad (4)$$

where $|A_1^i,B_2^j\rangle = \psi_i(\mathbf{r}_1-\mathbf{R}_A)\psi_j(\mathbf{r}_2-\mathbf{R}_B)$. Here A and B refer to the two nuclei locations, i and j refer to the single donor electronic states, 1 and 2 refer to the two electrons, and only one of the spin triplet is shown. Normalization and symmetry define the u and v coefficients. The two lowest eigenstates are singlet and triplet states obtained from the single donor ground state $i = j = A_1$. Their splitting $J(\mathbf{R})$ defines the Heisenberg exchange coupling between the ground-state donor electrons [see inset (b) in Fig. 1], and is a direct measure of the degree of control achievable over the entangled electronic states given in (4). When the initial state $|0\rangle$ is a singlet or a triplet with $i = j = A_1$, the lowest Raman-active final states $|f\rangle$ are obtained for $i = A_1$ and $j = E^{(\kappa)}$, where $\kappa = 1, 2$ refer to the two doublet states whose degeneracy has been lifted due to the axial perturbation of the donor pair.

There are 2 initial and 8 final states for Raman scattering from a donor pair in the $1S$ manifold. The 16 possibilities reduce to 4 Raman active combinations due to the absence of spin transitions (we neglect spin-orbit interactions) and the $A \leftrightarrow B$ symmetry of the HL state (4): Two of type $\{|0\rangle_s, |f^{(\kappa)}\rangle_s^+\}$ and two of type $\{|0\rangle_t, |f^{(\kappa)}\rangle_t^-\}$, $\kappa = 1, 2$. The superscript $\pm$ indicates $u = \pm v$ in (4).

The Raman allowed lines are schematically represented in the inset (b) of Fig. 1, and their calculated values for a substitutional impurity pair positioned along the [100] direction are given in Fig. 1, where triangles (squares) label singlet (triplet) lines, and open (filled) symbols correspond to $\kappa = 1(2)$. The behavior of the calculated Raman shifts in Fig. 1 illustrates general trends obtained for any orientation of $\mathbf{R}$, namely the overall convergence of all lines to the single-impurity value as $|\mathbf{R}|$ increases, superimposed with an oscillatory behavior (more apparent for $\kappa = 1$ for this particular direction) due to intervalley electronic interference of Si conduction band minima [8, 9]. In general, Raman transition energies are anisotropic and very sensitive to the relative positioning of the donor pair.

The propagation and polarization directions of the laser and Raman-scattered light, as well as the sys-

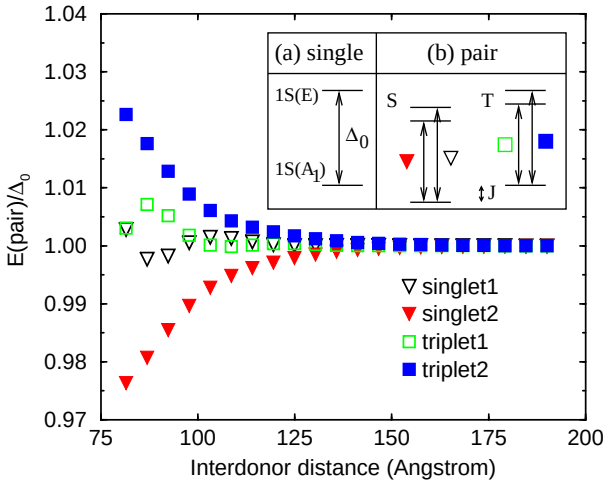

FIG. 1: Raman shifts of the four active transitions for a pair of substitutional donors placed along the [100] direction in Si, relative to the single impurity value Δ_0. Different symbols are defined in inset (b) and in the text. Insets: (a) Energy levels of a single P donor in Si leading to a Raman shift $\Delta_0 = 105$ cm^{-1}. (b) Schematic representation of the two-electron states of a P donor pair that participate in the Raman process.

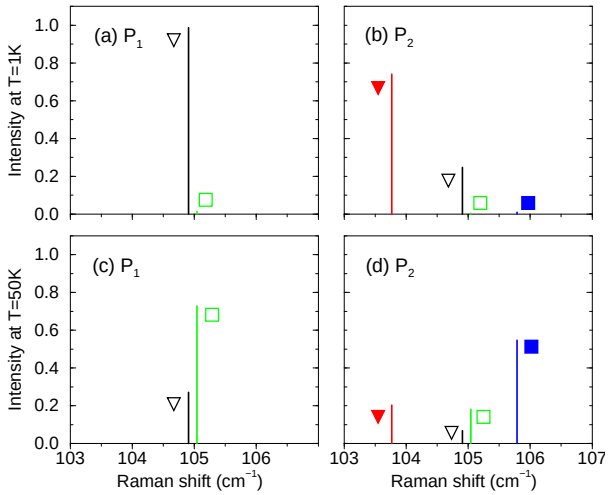

FIG. 2: Polarization and temperature effects in the Raman spectrum of an impurity pair separated by ~ 100 Å along [100]. Each vertical line represents a δ-function with weight (line intensity) proportional to its length. Frames (a) and (c) correspond to polarization P_1, parallel to $\mathbf{R}$, and (b) and (d) to polarization P_2, perpendicular to $\mathbf{R}$. Temperatures are as indicated on the left.

tem temperature, are controllable parameters in experiments. The usual notation to indicate the polarization scheme is $P = \vec{k}_L(\vec{\eta}_L, \vec{\eta}_R)\vec{k}_R$. Here we have considered the following: $P_1 = Z(X,X)\bar{Z}$, $P_2 = Z(Y,Y)\bar{Z}$, $P_3 = Z([110],[1\bar{1}0])\bar{Z}$ and $P_4 = Z([110],[110])\bar{Z}$, where X, Y, Z are the crystal axis [100], [010] and [001]. The relative Raman intensity of the different lines in a single spectrum is strongly dependent on the polarization components [see Eq.(2)]. We also consider temperature effects in the populations of the initial states $|0\rangle_s$ and $|0\rangle_t$, assumed to be in thermal equilibrium, i.e.

$$n_t/n_s = 3\exp(-J/k_BT)\,. \qquad (5)$$

In Fig. 2 we illustrate the combined polarization and temperature effects in the Raman spectrum for a pair of substitutional P donors along the [100] axis separated by ~ 100 Å(18 lattice parameters). Frames 2(a) and 2(b) are the data for low temperature ($T = 1$K), while frames 2(c) and 2(d) are high temperature data ($T = 50$K). In addition, frames 2(a) and 2(c) refer to polarization P_1, i.e., along $\mathbf{R}$. Here only two lines appear, because the $\kappa = 2$ lines (solid symbols in Fig. 1) yield $M = 0$ for P_1. The spectrum becomes more interesting for polarization P_2, perpendicular to $\mathbf{R}$, shown in frames 2(b) and 2(d). Here all four lines contribute to the spectrum. At low temperatures [frames 2(a) and 2(b)], practically all of the spectral weight is concentrated in the singlet lines, while for $T = 50$ K [frames 2(c) and 2(d)] all lines contribute, and the triplet lines are almost 3 times stronger than the corresponding (same κ) singlet lines due to the triplet spin degeneracy. Polarizations P_3 and P_4 lead to Raman lines qualitatively similar to P_2, but with reduced total intensity. We find that Raman intensities are stronger for polarization configurations such that $\vec{\eta}_L$ and $\vec{\eta}_R$ are either parallel or perpendicular to the relative position vector $\mathbf{R}$ (such as P_1 and P_2 in the present case of $\mathbf{R}$ along [100]), a feature that can be explored experimentally to determine the pair orientation.

In Fig. 3 we present the individual line intensities for increasing temperatures. The intensity of same-κ-pairs of singlet-triplet lines undergo a crossover close to the temperature J/k_B, a result easily obtained from Eq. (5). Thus J may be quantitatively estimated from the temperature dependence of the Raman line intensity. For $J \ll k_BT_{\min}$, the lowest experimentally achievable temperature, no effect should be observed by raising T, thus providing an upper bound for the value of J.

We have also investigated the Raman signature of an ensemble of donor pairs, which is within the current experimental capability. We consider a sample with an *ensemble of donor pairs* of average relative position $\mathbf{R}_0 = 100$ Åalong [100]. For each pair, with a given $\mathbf{R}_B$, $\mathbf{R}_A$ varies over all possible fcc lattice sites within a sphere of radius 10 Åcentered at $\mathbf{R}_B + \mathbf{R}_0$. The resulting spectra are given in Figs. 4(a) and 4(b). The Raman signature with polarization P_2 shows an interesting T dependence: as T increases, the spectral weight shifts upward in frequency, so that a low-energy shoulder at $T = 1$K becomes

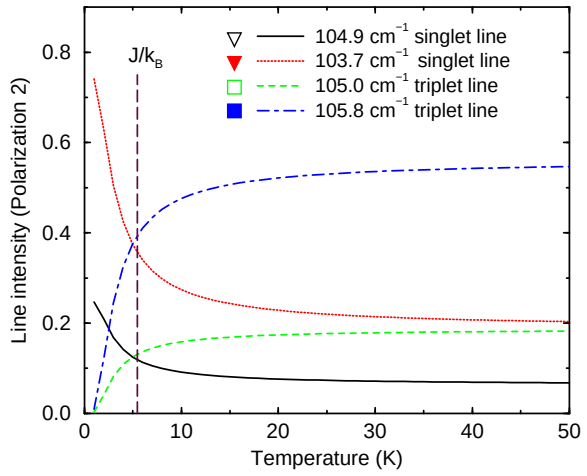

FIG. 3: Relative intensities of the Raman lines of an impurity pair for which the exchange coupling is $J = 0.47$ meV. Note that there is a crossover between singlet and triplet pairs at a temperature close to J/k_B, allowing to extract quantitative information about J

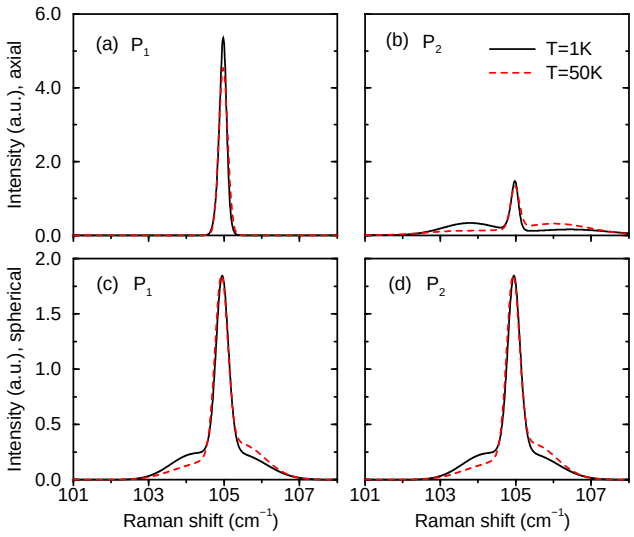

FIG. 4: Raman signature of non-Poissonian distribution of donor pairs. In panel (a) and (b) the pair distribution has axial symmetry, while in (c) and (d) the symmetry is spherical.

a high-energy shoulder at $T = 50$K. Our results thus show that conventional Raman experiments may be useful in identifying whether non-Poissonian axial distributions of donor pairs were actually achieved. Figs. 4(c) and 4(d) give results for a different type of pair distribution, also of average relative position $|\mathbf{R}_0|$, but with spherical symmetry: $\mathbf{R}_A$ varies over all possible fcc lattice sites between two spherical shells of radii $|\mathbf{R}_0 \pm 10|$ Åcentered at $\mathbf{R}_B$. Here the Raman signatures of the two polarizations are essentially identical, reflecting the sample's isotropic nature.

In this Letter we have proposed and analyzed a powerful and novel optical technique for disentangling donor exchange coupling information in the Si QC architecture. Our proposed technique actually transcends the specific problem (i.e. Si QC architecture fabrication) that motivated us–the proposed micro-Raman spectroscopic technique has the potential of becoming a versatile diagnostic tool in nanofabrication in general, since it can provide precise spatial information about relative positioning and entanglement of neighboring atoms in a host material, something that is very hard to do with any currently existing tools in solid state physics.

We thank LPS, ARDA and NSA for financial support, and Danilo Romero for useful conversations. BK also acknowledges financial support from CNPq (Brazil).

* Present address.
[1] C.H. Bennett and D.P. DiVincenzo, Nature **404**, 247 (2000).
[2] B.E. Kane, Nature **393**, 133 (1998).
[3] R. Vrijen *et al.*, Phys. Rev. A **62**, 012306 (2000).
[4] B.E. Kane, Fortschr. Phys. **48**, 1023 (2000).
[5] D. Mozyrsky, V. Privman, and M.L. Glasser, Phys. Rev. Lett. **86**, 5112 (2001).
[6] J. Levy, Phys. Rev. A **64**, 052306 (2001).
[7] J.L. O'Brien *et al.*, Phys. Rev. B **64**, 161401(R) (2001).
[8] B. Koiller, X. Hu, and S. Das Sarma, Phys. Rev. Lett. **88**, 027903 (2002).
[9] B. Koiller, X. Hu, and S. Das Sarma, cond-mat/0112078. Phys. Rev. B **66**, 115201 (2002).
[10] C. Tahan, M. Friesen, and R. Joynt, Phys. Rev. B **66**, 035314 (2002); M. Friesen *et al.*, cond-mat/0204035.
[11] R. de Sousa and S. Das Sarma, Phys. Rev. B **67**, 033301 (2003).
[12] D.N. Jamieson et al, in "Experimental Implementation of Quantum Computation", ed. by R.G. Clark (Rinton, Princeton, 2001), p 168.
[13] *Raman Microscopy*, ed. by G. Turrell and J. Corset (Academic Press, San Diego, 1996).
[14] Infrared absorption into optically-active levels [15] can be another useful tool in studying donor coupling in Si. However, the lack of any resonant enhancement severely limits the resolution of such an experiment.
[15] A.J. Mayur et al, Phys. Rev. B **48**, 10893 (1993).
[16] P.J. Colwell and M.V. Klein, Phys. Rev. B **6**, 498 (1972); K. Jain, S. Lai, and M.V. Klein, *ibid.* **13**, 5448 (1976).
[17] W. Kohn, in *Solid State Physics* **5**, ed. by F. Seitz and D. Turnbull (Academic Press, New York, 1957), p 257.
[18] L.X. Benedict et al, Phys. Rev. B **57**, R9385 (1998) reported excitonic effects in pure Si optical absorption. Excitonic effects in the intermediate state of the Raman process may sharpen the resonance, as the resonance enhancement factor would then be limited only by the inverse lifetime width of the exciton bound to the neutral donor.